10-2019

# Possible Detection of Low Energy Solar Neutrons Using Boron Based Materials

Nicole Benker
*University of Nebraska - Lincoln*

Elena Echeverria
*University of Nebraska - Lincoln*

Robert Olesen
*Air Force Institute of Technology*

Brant E. Kananen
*Air Force Institute of Technology*

John W. McClory
*Air Force Institute of Technology*

*See next page for additional authors*



## Recommended Citation

Benker, N., Echeverria, E., Olesen, R. J., Kananen, B. E., McClory, J. W., Burak, Y., Adamiv, V. T., Teslyuk, I., Peterson, G. G., Bradley, B., Wilson, E. R., Petrosky, J. C., Dong, B., Kelber, J., Hamblin, J., Doumani, J., Dowben, P. A., & Enders, A. (2019). Possible detection of low energy solar neutrons using boron based materials. Radiation Measurements, 129, #106190. https://doi.org/10.1016/j.radmeas.2019.106190

# Possible Detection of Low Energy Solar Neutrons Using Boron Based Materials

Nicole Benker[1], Elena Echeverria[1], Robert Olesen[2], Brant Kananen[2], John McClory[2], Yaroslav Burak[3], Volodymyr Adamiv[3], Ihor Teslyuk[3], George Peterson[2,4], Ben Bradley[4], Ethiyal R. Wilson[1], James Petrosky[2], Bin Dong[5], Jeffry Kelber[5], Jennifer Hamblin[1], Jacques Doumani[1], Peter A. Dowben[1], and Axel Enders[1,6]

[1]Department of Physics and Astronomy, Jorgensen Hall, 855 North 16 Str., University of Nebraska –Lincoln, Lincoln Nebraska 68588-0299
[2]Department of Engineering Physics, Air Force Institute of Technology, 2950 Hobson Way, Wright-Patterson AFB, Ohio 45433-7765
[3]Institute of Physical Optics, 23 Dragomanov Str., Lviv 79-005, Ukraine
[4]Department of Mechanical and Materials Engineering, Nebraska Hall, University of Nebraska – Lincoln, Lincoln Nebraska 68588-0526
[5]Department of Chemistry, University of North Texas, 232 Science Research Bldg., Ave. B and Mulberry Streets, Denton, Texas 76203-5017
[6]Physikalisches Institut, Naturwissenschaften I, Universität Bayreuth, Universitäts Strasse, Bayreuth, Bavaria, Germany

*Key words:* Helio astronomy particle emission; detector instrumentation; space vehicle instruments; Helio nucleosynthesis

*Correspondence to:*

Peter A. Dowben
Department of Physics and Astronomy
Theodore Jorgensen Hall
855 North 16th Street
University of Nebraska-Lincoln
Lincoln, NE 68588-0299
E-mail: pdowben1@unl.edu
+1-402-472-9838

## ABSTRACT

Solar neutrons have been detected aboard the International Space Station (ISS), using lithium tetraborate and boron carbide detector elements. We find that evidence of low energy solar neutron flux, as detected in a neutron calorimeter following subtraction of the proton background, is consistent with Monte Carlo simulations that suggest an energy of about 1 to 2 MeV. This solar neutron flux is likely no more than 250 to 375 neutrons $cm^{-2}sec^{-1}$, with a lower bound of 50 to 75 neutrons $cm^{-2}sec^{-1}$ at one au.

## 1. INTRODUCTION

The existence of solar neutrons entering the near-Earth environment has long been predicted (Biermann, Haxe & Schulter 1951) but several years and many attempts were required before experimental confirmation was achieved (Chupp et al. 1982; Forrest et al. 1982). While Biermann et al. predicted a solar neutron flux energy in the region of 10 MeV or higher, these expectations have yet to be thoroughly investigated. The detection of low energy solar neutrons in the range of 0.5–7.5 MeV, at 0.48 au, by the MESSENGER Neutron Spectrometer, have been reported (Feldman et al. 2010; Lawrence et al. 2014) and were associated with a solar flare event. The latter results have been heavily criticized (Share et al. 2015). The core argument against the assignment of 0.5–7.5 MeV detected, as solar neutrons, was that the MESSENGER neutron spectrometer could not distinguish between secondary neutrons produced by particle interactions in the spacecraft and a direct solar neutron flux (Share et al. 2015). With regard to the detection of higher energy solar neutrons (i.e. much greater that 20 MeV), there are a wide number of experimental observations. The most significant energetic solar neutron events observed can now be associated with solar flares (Chupp et al. 1982, 1987; Holman 2000; Kuznetsov et al. 2006, 2011; Masuda et al. 1994; McConnell et al 1993; McConnell 1994; Murphy et al. 1999; Muraki & Shibata 1996; Muraki et al. 2012; Petschek 1964; Rank et al. 1996; Ryan et al. 1994; Ryan & McConnell 1996; Ryan 2000; Shea, Smart & Pyle 1991; Shibata 1998; Yokoyama & Shibata 1998). A solar neutron scintillation detector was designed and launched in 2009 as an attached payload to measure radiation levels aboard the International Space Station (ISS) (Koga et al. 2001, 2011; Muraki et al. 2012). The lowest neutron energy that can be measured by this detector, however, is 35 MeV, far above the neutron energies generated from many potential solar nucleosynthetic processes, for instance D-D, D-T and D-Li fusion reactions (Hoyle 1946, 1954). To measure the low energy, possibly steady state, solar neutron flux, a different type of detector design is required.

Detection of the low energy solar neutron flux is far from trivial. Neutrons of 1 MeV kinetic energy travel at speeds of approximately $1.38\times10^{7}$ m $s^{-1}$ (roughly 5% the speed of light), or transverse 1 au in about 3 hours. The unbound neutron lifetime is approximately 15 min (881.5±8 s) before decay, via the weak interaction, to a proton, an electron, and an antineutrino. This means that nearly all of the slow unbound solar neutrons produced decay before arriving at Earth. Only a tiny fraction of the low energy neutrons surviving the 1 au journey: for 1 MeV neutrons, the resulting exponential decay means that only approximately $4.6x10^{-6}$ survive. Unlike electrons and protons, neutrons can pass through large amounts of material without being scattered or absorbed. Additionally, a significant

signal must be reliably detected above a significant background. This background includes neutrons generated by cosmic rays and other sources, which combined, makes the detection of a low energy solar neutron flux at the surface of the earth very difficult. Since a low energy solar neutron flux will essentially nearly completely decay at 1 au, if the resulting proton production is then indistinguishable from the solar wind, this implies a neutron energy of 800 to 900 eV. At the surface of the Earth, the low energy solar neutron flux is further diminished by scattering and absorption in the atmosphere making it difficult to distinguish from the secondary neutron background flux. For this reason, effective measurement of low-energy solar neutrons requires a space-based detector.

The ideal neutron detector is gamma blind, robust, and lightweight, using low-Z elements with a high neutron cross-section. For these reasons, lithium and boron containing materials are favored over detectors employing higher-Z elements like cadmium, gadolinium, uranium, and plutonium as well as well as gas-based detectors that rely on increasingly scarce helium 3 ($^3$He). Detector elements based on neutron capture by $^6$Li and $^{10}$B requires the neutrons to be thermalized, as the neutron capture cross-section by $^6$Li and $^{10}$B is only significant for energies below 40 meV (for a review see (Caruso 2010)). Therefore, a significant moderator is required to enable neutron capture of the incident solar neutrons at energies above 1 MeV, to improve the efficiency of detectors based on $^6$Li and $^{10}$B (Caruso 2010).

Stacking multiple detector elements between moderator layers provides an indication of the incident neutron's energy. The total moderation is small enough that highly energetic solar neutrons, associated with solar flares, will pass through undetected, while the lower energy neutrons become moderated enough to be captured by the $^6$Li and $^{10}$B. By using a layered series of moderator material and detector elements, an assessment of the neutron energy is possible through construction of a neutron calorimeter or spectrometer (Caruso 2010, Bramblett, Ewing & Bonner 1960, Hoshor et al. 2015, 2017). Determining directionality of the flux is also possible - secondary neutron flux from cosmic ray generated neutrons on the nadir side (entering the detector from the Earth facing side) can be distinguished from low energy neutrons approaching the detector from the zenith (sun facing side), as discussed below (*vide infra*).

## 2. MATERIALS AND METHODS

Preliminary studies by this team using a high-altitude NASA balloon to investigate lithium hexaborate ($Li_2B_6O_{10}$) glass detector elements demonstrated that we can detect neutron fluences in the low neutron energy limit, at very high altitudes. Since the detector elements were glass, they were not particularly sensitive to increases in local disorder due to the amorphous internal structure. The fact that increased disorder was detected in an amorphous material (see appendix I) indicates that lithium borate materials are very good candidates for neutron detector elements. Lithium borate materials, if crystalline, are thus more sensitive to radiation damage and more suitable for neutron detection at low flux and low neutron energies. The University of Nebraska detector for the analysis of solar neutrons (DANSON) system was flown aboard the International Space Station (ISS), at a significantly higher altitude, and used three types of lithium tetraborate ($Li_2B_4O_7$) single crystal detector elements. These three types of detector elements included lithium tetraborate crystals with a natural abundance of $^{10}$B (approx. 20% $^{10}$B, 80% $^{11}$B,

designated as LTB-N for the rest of this paper), crystals enriched in $^{10}B$ (for what follows, designated as LTB-10), and crystals enriched in $^{11}B$ (for what follows, designated as LTB-11). $^{10}B$ enrichment in lithium tetraborate provides a higher cross section for thermal neutron capture, while crystals enriched in $^{11}B$ create a detector element with negligible cross section for thermal neutron capture, while maintaining a proton capture cross section comparable to that of $^{10}B$. The radiation signatures in the $^{11}B$ enriched elements (LTB-11) were used in the subtraction of the proton flux in order to more accurately assess the low energy solar neutron flux and mean neutron energies at one astronomical unit from the sun.

The presence of imperfections within the lithium tetraborate crystals mandates the use of control elements in addition to simply comparing the intensities of exposed elements. The Harshaw thermoluminescence reader produced a thermoluminescence glow curve for the lithium tetraborate single crystal detector elements exposed to solar neutrons aboard the International Space Station (ISS). Upon return of the experiment from NASA, the thermoluminescence curves for the crystal detector elements were compared to not-flown natural abundance and $^{10}B$ enriched lithium tetraborate crystals used as control elements. This established that there was increased radiation damage aboard the ISS. The resulting thermoluminescence glow curve for each crystal was summed from 100 ℃ to 230 ℃. This was done to minimize the impact of random noise in each thermoluminescence glow curve. This sum was then divided by the mass of each crystal to correct for slight variations in crystal volume. The glow curve sum of the LTB-11 detector elements was subtracted from the proton plus neutron composite signal of the ISS flown companion LTB-N and the LTB-10 detector elements. This difference in the thermoluminescence intensity between the LTB-10 detector elements ($I_E$) and LTB-11 control elements ($I_0$) should be proportional only to the solar neutron flux, i.e.

$$[(I_E(^{10}B\ enriched) - I_E(^{11}B\ enriched)) - (I_0(^{10}B\ enriched) - I_0(^{11}B\ enriched))] \quad (1)$$

Thermoluminescence, photoluminescence, photoluminescence excitation, and electron paramagnetic resonance experiments were carried out on various the lithium tetraborate ($Li_2B_4O_7$) single crystal detector elements. Thermoluminescence data was collected using a Harshaw 3500 TLD Reader with a 1 ℃ $s^{-1}$ heating rate under flowing nitrogen gas. A Horiba Fluorolog-3 spectrometer was used to obtain the photoluminescence and photoluminescence excitation data. This spectrometer has a xenon lamp as the excitation source, a Hamamatsu R928 photomultiplier as a detector, and two double-grating monochromators to measure emission and excitation spectra. The photoluminescence showed a clear feature at 370 nm and photoluminescence excitation provided a peak at 270 nm, which combined, indicates the presence of copper impurities, which can be compared to photoluminescence features indicative of Cu (Patra et al. 2012, 2013, Rawat et al. 2012). Both the natural abundance and $^{10}B$ enriched lithium tetraborate crystals both showed evidence of copper impurities, as have been seen elsewhere (Brant et al. 2013; Tiwari et al. 2010). The thermoluminescence glow curve, for the reference lithium tetraborate sample crystals, taken after room temperature X-ray irradiation, yielded two thermoluminescence peaks at 120 ℃ and 240 ℃. Both of these peaks are also indicative of copper impurities. The lack of copper related electron paramagnetic resonance spectra after X-ray irradiation indicates that the level of copper impurities

is low in the lithium tetraborate single crystal detector elements.

There is an increased thermoluminescence signature, in the lithium tetraborate crystal detectors elements, that arises due to damage to the crystal structure when $^{10}B$ neutron capture occurs. This neutron capture process results in the loss of boron and creation of daughter fragments with significant kinetic energy. The relevant neutron capture processes are:

$$^{10}B + n \rightarrow {}^{7}Li\ (0.84\ MeV) + {}^{4}He\ (1.47\ MeV) + \gamma\ (0.48\ MeV)\ (94\%)\quad (2)$$

$$^{10}B + n \rightarrow {}^{7}Li\ (1.02\ MeV) + {}^{4}He\ (1.78\ MeV)\ \ (6\%)\quad (3)$$

the neutron capture reactions

$$^{10}B + n \rightarrow {}^{9}Be + {}^{2}H \qquad (4)$$

$$^{10}B + n \rightarrow {}^{10}Be + {}^{1}H \qquad (5)$$

have negligible cross by comparison but would also create significant damage tracks within the crystal.

Additionally, the experiment used semiconducting heterojunction diode detector elements of n-type Si(100) to hydrogenated boron carbide ($B_{10}C_2H_X$) alloyed with pyridine moieties, and n-type Si(100) to hydrogenated boron carbide ($B_{10}C_2H_X$) alloyed with benzene moieties to create semiconducting heterojunction diodes (the latter denoted hereafter as boron carbide heterojunctions). The fabrication of the plasma enhanced chemical vapor deposited (PECVD) hydrogenated boron carbide ($B_{10}C_2H_X$) alloyed with pyridine moieties on n-type silicon have been well described elsewhere (Echeverria et al. 2016). These heterojunction diode characteristics are sensitive to neutron capture induced damage, unlike the PECVD boron carbides without aromatic moiety constituents (Peterson et al. 2018). These boron carbide heterojunction detectors also make use of the high $^{10}B$ neutron capture cross-section and provide a means of measuring the flux.

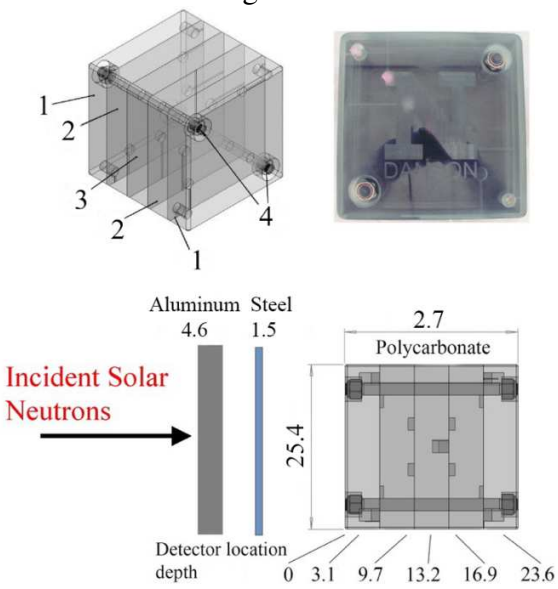


***Figure 1.*** *Schematic of the Makrolon™ plate assembly for the DANSON detector. The 7075-T7 aluminum alloy, and 304 stainless steel are from the skin of ISS and zenith side hatch, as indicated at bottom left. The end plates (1), side plates (2), center plate (3) and locking bolts (4) are indicated, in the schematic on the left. The detector elements are placed in the pockets cut into the plates, located along the main diagonals of the cube. The assembled solar neutron detector is shown at right. When placed aboard ISS Node 2 Zenith, the zenith side of the DANSON detector is behind 4.6 cm of aluminum and 1.5 cm of steel as indicated. All thickness and depth dimensions are in cm.*

Similar to the lithium tetraborate detector elements, the radiation signature in the boron carbide diodes occurs as a result of neutron capture by $^{10}B$. The boron carbide heterojunction diode detector elements were analyzed for changes in detector response via capacitance versus voltage, C(V), and current versus voltage, I(V), measurements. The electronic characteristics of these devices were then compared to measurements taken on the same samples prior to being flown on ISS. In the case of

these boron carbide heterojunction detector elements, we find that under moderate neutron irradiation the diode characteristics are degraded, and the extent of degradation can be compared against a series of samples exposed to known neutron fluxes. The degradation appears as an increase in reverse bias leakage current, and an increase in series resistance across the device.

The detector elements were surrounded by impact resistant polycarbonate Makrolon™ (a thermoplastic polymer) to slow the energetic incident neutrons to epithermal energies (30 meV or lower) where, as noted above, the neutron capture cross-section of both $^{6}$Li and $^{10}$B is high (Caruso 2010). The neutron capture cross-section for $^{10}$B at energies above 30-40 meV is extremely small, falling to less than 2 barns at 1 eV, even less for $^{6}$Li (Caruso 2010, Chadwick et al. 2006).

The five LTB-N, five LTB-10, and five LTB-11 detector elements were encased within volumes milled into slabs of the Makrolon™ polymer, at various depths along two main diagonals of the cube to prevent detector element overlap and to allow for variations in the extent of neutron thermalization resulting from varying thicknesses of moderator material, as indicated in Figure 1. Thus, the higher the neutron energy, the greater penetration into the Makrolon™ cube, say from the zenith face, before sufficient moderator is encountered to slow the neutron energies for a neutron capture event to occur. This provides a crude neutron calorimeter or spectrometer, much as described by (Caruso 2010, Bramblett et al. 1960, Hoshor et al. 2015, 2017), again as noted above.

The LTB-N, LTB-10, and LTB-11 detector elements were each placed at depths of 3.1, 9.7, 13.2, 17.0, and 23.6 cm from the zenith face of the Makrolon™ cube, as summarized in Table 1. This means that each LTB-N, and LTB-10 detector element has a companion LTB-11 detector element for proton and other radiation background subtraction. The boron carbide heterojunction detector elements were placed at depths of 3.1 cm and 17.0 cm from the zenith face of the Makrolon™ cube.

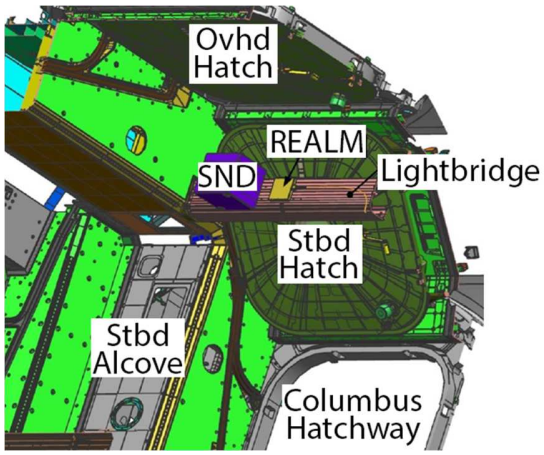


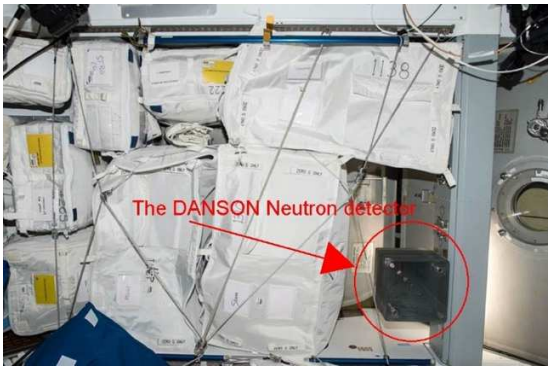


***Figure 2.*** *The DANSON detector payload location, labelled SND (top) in the payload topology forum rendering for the International Space Station (ISS) Node 2 Zenith. At the bottom, the actual detector cube is shown affixed to the light bridge structure running between the starboard and overhead hatches on the zenith side of ISS Node 2 (Harmony) module of the ISS. Its facing was to the overhead (zenith) hatch. It was surrounded on three sides by cargo stowage bags filled with crew laundry and the on the fourth side by the Columbus module.*

The placement of the DANSON detector cube at Node 2 Zenith, aboard ISS, ensured that as little as possible of the neutron signal

was diminished by materials within the station. Additionally, the directionality was enhanced by surrounding non-zenith facing sides of the detector with hydrocarbon-dense heterogenous organic materials (crew clothing stowage), as seen in Figure 2 (at the bottom).

Table 1: Placement of the Detector Elements

| Layer # | Distance from Zenith Side (cm) | Detector elements |
|---|---|---|
| 1 | 3.1 | LTB-10<br>LTB-N<br>LTB-11<br>Boron Carbide Diode |
| 2 | 9.7 | LTB-10<br>LTB-N<br>LTB-11 |
| 3 | 13.2 | LTB-10<br>LTB-N<br>LTB-11 |
| 4 | 17.0 | LTB-10<br>LTB-N<br>LTB-11<br>Boron Carbide Diode |
| 5 | 23.6 | LTB-10<br>LTB-N<br>LTB-11 |

## 3. DETECTION OF SOLAR NEUTRONS

The DANSON payload was launched on the OA-5 Commercial Resupply Services mission on 2016 October 17 at 23:45 UT, docking to ISS on October 23 at 14:53 (the delay in docking was due to a Soyuz craft arrival shortly after the OA-5 launch and Cygnus orbital insertion). The experiment was deployed to Node 2 (Figure 2), on ISS at approximately 14:30 on October 27. The detector package (including moderator layers) was restowed approximately 15:25 on 2017 March 17, returning on SpX-10 Dragon craft, with undock at 09:11 and splashdown at 14:46 on 2017 March 19. The estimated total solar exposure time during deployment is $8.02 \times 10^6$ s.

The proton signal from the LTB-11 detector elements was subtracted from the proton plus neutron composite signal of the natural abundance elements and the LTB-10 detector elements. After the lithium tetraborate thermoluminescence signal, created by the proton flux, has been subtracted out, as discussed above, we have an estimate of what moderation is needed for good neutron capture, as seen in Figure 3. Similar normalization was also done for the LTB-N detector elements, also as plotted in Figure 3.

The stronger thermoluminescence signal, after proton flux background subtraction, was towards the zenith side, for both sets of lithium tetraborate samples, as seen in Figure 3. Backscattered proton flux from the van Allen belts or a cosmic ray generated neutron flux should be more predominantly evident in the detector assembly at the nadir side (Layer #5 in Figure 3). Because the stronger neutron signatures are at the zenith side, not nadir side, we must conclude that at least some of

***Figure 3.*** *The neutron capture signal, taken from the thermoluminescence glow curve, as a fraction of total signal following proton background subtraction. Blue curve: LTB-10 detector element signal less the signal LTB-11 detector element; red curve: the difference between the intensity from LTB-N detector elements and LTB-11 detector elements, rescaled to correct for diminished $^{10}B$ (red curve). The negative thermoluminescence intensity, in the data from the natural abundance of boron isotopes crystal intensities, arises from the LTB-11 background subtraction where, after rescaling, there is more signal from the proton background than from the neutron flux. Layer placement, i.e. distance from zenith side, is summarized in Table 1, so layer #1 is zenith side and layer #5 is nadir side.*

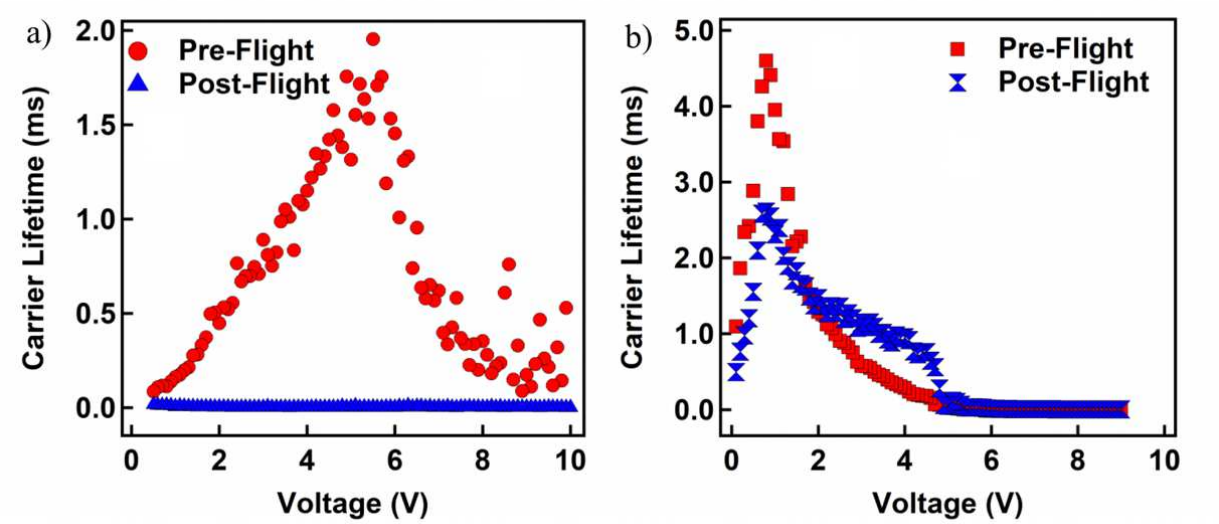


***Figure 4.*** *The changes in measured drift carrier lifetimes for n-type Si(100) to PECVD semiconducting boron carbide heterojunction diode detectors whose device characteristics before (red) and after (blue) space flight have been compared, for (a) layer 1 (zenith side) and (b) layer 4 (nadir side).*

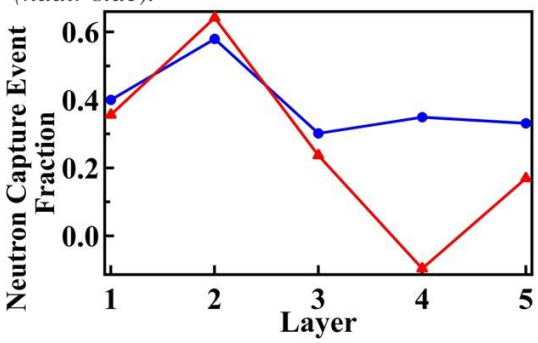


the neutron signature must be the result of a low energy solar neutron flux, not back scattered cosmic ray neutrons, nor neutrons from the van Allen belts and below (i.e. nadir side). While there is some indication enhanced neutron detection on the nadir side, for one set of data, i.e. for the LTB-N data of layer 5 (Figure 3), this was not reproduced in both sets of lithium tetraborate data, appearing only in the set of data with lower neutron cross-section.

Although less compelling, greater radiation damage is also evident in the greater decrease in the estimated drift carrier lifetimes at the zenith side versus the nadir side, seen in the boron carbide heterojunction detector elements. The changes in the combined I(V) and C(V) characteristics allows us to infer (as indicated in appendix II) a vastly reduced drift carrier lifetime, by several orders of magnitude, in the boron carbide heterojunction detector elements, on zenith side (Figure 4a), compared to only a 40% to 50% reduction in drift carrier lifetime for similar detector elements placed more towards the nadir side, as plotted in Figure 4b. The boron carbide heterojunction detector elements fabricated from orthocarborane and benzene precursors is particularly susceptible to radiation damage and it is this type of detector element, on the zenith side, that shows the most damage as indicated by the vastly reduced drift carrier lifetime.

### 3.1. The Mean Energy of the Low Energy Solar Neutron Flux

To obtain the mean energy of the solar neutron flux and to assess the significance of solar neutrons over all other neutron capture events, the proton flux must be subtracted as described. Because of high levels of hydrogen contained in the moderating Makrolon polymer material facilitating neutron thermalization, a variation in the

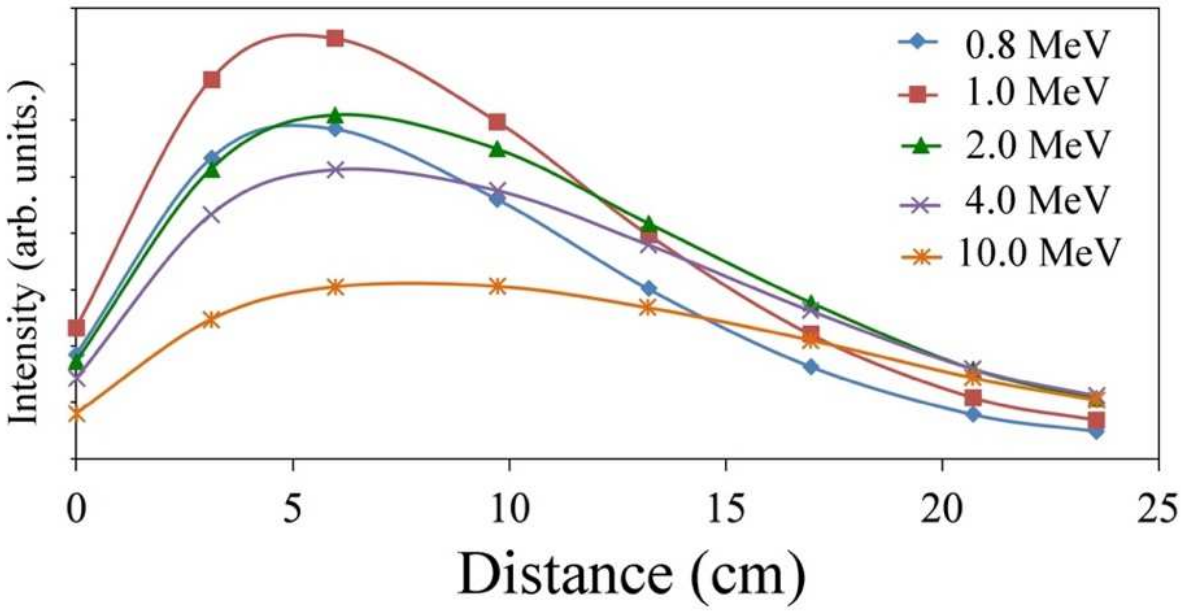


***Figure 5.*** *The predicted neutron capture distribution for neutrons of various incident energies, based on MCNP6, as a function of distance into the DANSON detector, taking also into account that the entire detector package is behind approximately 4.6 cm of aluminum and 1.5 cm of steel representing the ISS bulkhead and hatch between the detector package and the outside space environment.*

intensity of the neutron capture signatures with depth is expected, as noted above. The distribution of neutrons, which is determined by the variation in path lengths through the moderating plastic, must be unfolded or compared to simulations. Thus, assessing the mean neutron energy of the solar neutron flux requires Monte Carlo simulations, performed with MCNP6 (Goorley et al. 2012, Goorley et al. 2016) to aid in the analysis of the solar neutron distribution. The detector package and relevant portions of ISS Node 2 hatch and bulkhead (provided by NASA), as indicated in Figures 1 and 2, were modeled using MCNP6 to estimate the neutron flux throughout the detector package. The normalized flux of neutrons below 40 meV (to which the detector crystals are most sensitive) versus depth into the DANSON detector is plotted in Figure 5 for various incident neutron energies. The penetration of neutrons into the detector package was also evaluated using GEANT4 (Agostinelli et al. 2003, Allison, J., et al., 2006, Allison, J., et al., 2016) and similar results were obtained. The moderating effects of aluminum, steel, and polymer, as indicated in Figures 1 and 2, were included in the MCNP6 simulations summarized in Figure 5.

As is evident, neutron energies well below 500 keV would lead to the neutron capture signature being greatest at Layer 1, in Figure 3. Incident neutron energies above 10 MeV would lead to the neutron capture signature being fairly uniform with depth onto the DANSON detector. The best fit of the Monte Carlo simulations (Figure 5) to the experimental data (Figure 3) is, however, for neutron energies between 1 to 2 MeV, based on a modified least squares fit. We find very poor match between experiment and the extremes of the MCNP simulations, i.e. for 0.8 and 10 MeV neutron energies. This not what has been generally expected (Biermann et al. 1951), but consistent with the observation of 0.5–7.5 MeV solar neutrons detected at 0.48 au, by the

MESSENGER Neutron Spectrometer, and associated with a solar flare event (Feldman et al. 2010; Lawrence et al. 2014). We can also exclude neutrons produced by D-T reactions at the surface of the sun, as the

$$^{3}H + ^{2}H \rightarrow ^{4}Li\ (3.5\ MeV) + ^{1}n\ (14.1\ MeV) \quad (6)$$

reaction produces neutrons at far too high an energy to fit the results.

Cosmic-ray albedo neutrons, with kinetic energies of tens to hundreds of MeV (Li et al. 2017), would generally not have the detection profile observed in the DANSON detector, as at these high neutron energies, most neutrons would pass through the detector, as there is insufficient material to thermalize such high energy neutrons. The propagation of cosmic rays, through the Earth's atmosphere, does result secondary neutrons in the region of 1 to 3 MeV (Clem et al. 2004, Wiegel et al. 2002), but the neutron flux has been calculated and measured to be low, overall, with values of about 5 $cm^{-2}s^{-1}$ or less expected. While the DANSON detector might detect such neutrons, the placement on ISS, with insufficient depth in the Earth's atmosphere, makes detection of such neutrons unlikely, as this flux will be very low. There is also flux of secondary neutrons created by the materials aboard ISS, and while estimated to be less than 15 $cm^{-2}s^{-1}$, this is discussed in greater detail below.

### 3.2 The Low Energy Solar Neutron Mean Flux

To estimate the neutron flux, as indicated above, the device characteristics of boron carbide heterojunctions were assessed for damage induced by neutron capture, combined with the assessment of the total irradiation time estimated using Systems Tool Kit (STK), an orbital mechanics software, and public ISS orbital data provided by NASA for the mission dates. The n-type Si(100) to hydrogenated boron carbide, alloyed with aromatics, heterojunction diodes are particularly sensitive to the neutron capture induced damage, as noted at the outset. These types of boron carbide semiconducting heterojunction diodes were used in the DANSON detector as additional neutron detector elements. The I(V) characteristics of these boron carbide heterojunction diodes show the expected changes resulting from neutron damage, as seen in Figure 6. The amount of degradation evident in the I(V) characteristics, that is to say in the forward bias current regime, or series resistance, corresponds to about $3\times10^{9}$ neutrons $cm^{-2}$ exposure, based on prior calibration experiments. This estimate though does not

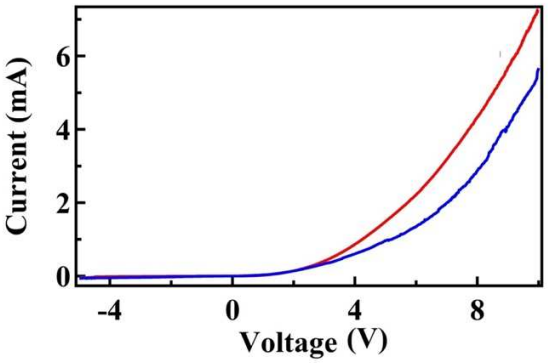


account for any corrections for radiation damage caused by the proton background, so is in fact a measure flux that include neutrons and protons.

***Figure 6.*** *The changes in measured I(V) characteristics for the boron carbide heterojunction detector elements, whose device characteristics before (red) and after (blue) space flight have been compared. These boron carbide heterojunction detector elements were designed to be particularly susceptible to radiation damage, but proton flux damage cannot be subtracted out and will contribute the device degradation.*

Since the estimated total solar exposure time for deployment is $8\times10^{6}$ s, this total radiation corresponds to about 250 to 375

neutrons and protons $cm^{-2}s^{-1}$, with a significant fraction of the measured damage (Figure 6) from the 1-2 MeV low energy solar neutron flux. Given the estimates of the proton flux damage (as described above, from analysis of the LTB-10, LTB-N and LTB-11 detector elements), relative to the damage from the composite flux of neutrons and protons combined, the incident 1-2 MeV low energy neutron flux is not less than 125 to 188 neutrons $cm^{-2}s^{-1}$.

By subtracting the neutron flux counts from the nadir side from zenith side, we can estimate that this means is that there are 50 to 75 neutrons $cm^{-2}s^{-1}$ that cannot be attributed to any background that may arise from secondary neutron production from the spacecraft structure or cosmic rays (cosmic-ray albedo neutrons). At a mean 2 MeV energy, for the neutrons detected, this corresponds to 1.96 x $10^7$ m $s^{-1}$, so that, by far, most of neutrons decay, at 1 au. From this decay, there are 8.4 x $10^5$ baryonic particles in the solar wind originating from solar neutrons, as decay products. At 1 au, the solar wind is ~2 × $10^8$ $cm^{-2}$ $s^{-1}$ in high-speed streams and ~4 × $10^8$ $cm^{-2}$ $s^{-1}$ (Feldman et al. 1978; Goldstein et al. 1996; Leer, Holzer & Flå 1982; Wang 2010), this means that 1.1% to 0.42%, perhaps more, of the baryonic solar wind was originally neutrons. For a solar wind speed that is approximately 4 x $10^5$ m $s^{-1}$, this small component of the baryonic solar wind, from neutrons, comes at a significantly higher velocity (in the region of 1.96 x $10^7$ m $s^{-1}$) as noted above.

## 4. SUMMARY

A neutron detector, constructed of different types of detector elements layered at varying depths within a body of moderating material, was flown aboard ISS to measure the slow solar neutron flux. Upon return, the neutron mean energy was extracted by unfolding the thermoluminescence glow curve responses of the $^{10}B$ enriched and natural abundance lithium tetraborate single crystal elements, as a function of moderator path length and subtracting the proton flux damage out using $^{11}B$ enriched lithium tetraborate single crystal elements. The neutron flux was extracted by analysis of changes in the device characteristics of alloyed hydrogenated boron carbide semiconducting heterojunction diodes. The directionality of the signal and location of the highest concentration of neutron capture events in both the lithium tetraborate single crystal detector elements and the boron carbide heterojunction diodes indicate detection of a nonzero low energy solar neutron flux. Through Monte Carlo simulations, this lower energy neutron flux was estimated to have a mean energy in the region of 1 to 2 MeV with a flux of more than 50 to 75 neutrons $cm^{-2}s^{-1}$, that is difficult to ascribe to secondary neutron production from the spacecraft structure or cosmic rays (cosmic-ray albedo neutrons). This is significant as unlike electrons and protons, neutrons can pass through large amounts of material without being scattered or absorbed.

## ACKNOWLEDGEMENTS

This work was supported by the National Aeronautics and Space Administration through grants NNX13AN16A, NNX14AL11A and NNX15AI09H and the Defense Threat Reduction Agency (Grant No. HDTRA1-14-1-0041). ERW was supported by Nebraska Public Power District through the Nebraska Center for Energy Sciences Research. GP was supported by the Office of Research and Economic Development at the University of Nebraska-Lincoln. Orbital modelling software STK was provided under an educational license from Analytical Graphics, Inc. The authors would like to thank Scott Whitehead (NASA), Glenn

Ferraro (NASA) and Scott Tarry (University of Nebraska at Omaha Aviation Institute) who have assisted in this project development as well as astronaut Shane Kimbrough (NASA) for his technical assistance aboard ISS.

## APPENDIX I

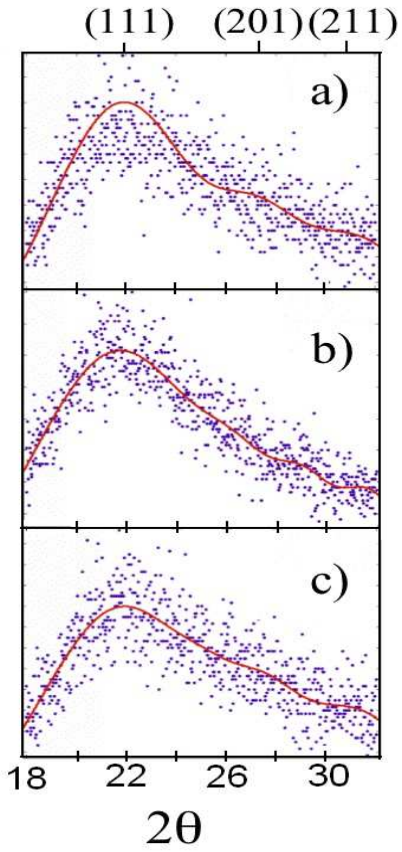


***Appendix Figure 1.*** *X-ray diffraction indicating the structure damage for neutron capture in $Li_2B_6O_{10}$ glass samples. While a glass, there is sufficient local short range order for some of the diffraction lines of the bulk single crystal to be apparent. These are indicated in the Figure as assigned to the appropriate Miller index. Bottom of figure shows horizontal axis with X-ray diffraction angle, top of figure shows horizontal axis with Miller indices, and vertical axis shows scattering intensity. Local short range order degradation, relative to the reference (a), is seen in the $Li_2B_6O_{10}$ glass samples exposed to high altitude epithermal neutrons (b), and samples moderated by Lexan™ to make then sensitive to hot high altitude 1-2 MeV neutrons (c). Damage is most apparent in (c), indicative of the greatest number of neutron capture*

Preliminary studies showed that detection neutron fluxes at very high altitudes was possible, and employed lithium hexaborate glasses. These measurements do not exclude secondary neutrons in the region of 1 to 3 MeV (Clem et al. 2004). The samples were tested in a high altitude NASA balloon. The basic advantage to this test was that such detector elements were low weight, low maintenance and robust. Two $Li_2B_6O_{10}$ glass samples were irradiated at modestly high altitude (roughly 84,000 feet above sea level). These samples were packaged differently, with one encased in Lexan™ to moderate the higher energy neutrons and increase neutron capture of higher energy (1-3 MeV) neutrons, and one exposed, without any moderator, thus sensitive to epithermal neutrons only. After sample recovery, the microstructure and optical properties of the $Li_2B_6O_{10}$ glass samples were analyzed and compared to a control sample kept isolated on the ground. The detector elements were a glass, and thus not very sensitive to increases in local disorder due to the amorphous internal structure, but damage from neutron or other radiation was, nonetheless, detected, as evident in the X-ray diffraction signature of increased disorder of the glass, as seen in Appendix Figure 1.

## APPENDIX II

The drift carrier lifetime, characteristic of our n-type Si(100) to hydrogenated boron carbide ($B_{10}C_2H_X$), alloyed with benzene moieties semiconducting heterojunction diode detector elements deposited by PECVD, was extracted from the C(V) and I(V) curves, as in (Echeverria et al. 2016, 2017; Ilie et al. 2018; Peterson et al. 2018), beginning from the I(V) data where the low frequency conductance, $G_0$, is given by:

$$G_0 = \mathrm{d}I/\mathrm{d}V_a, \quad (A1)$$

where $I$ is the measured current and $V_a$ is the applied bias in volts. The frequency dependent diffusion capacitance, $C_D$, is correspondingly given by:

$$C_D = (G_0/\omega\sqrt{2})\left(\sqrt{1+\omega^2\tau^2}-1\right)^{1/2} \quad \text{(A2)}$$

Where $\omega$ is the angular frequency ($2\pi f$), and $\tau$ is the drift carrier lifetime, or the effective carrier lifetime. The drift carrier lifetime $\tau$ can then be extracted as:

$$\tau = \sqrt{\frac{\left(2C_D^2\omega^2/G_0^2+1\right)^2-1}{\omega^2}} \quad \text{(A1)}$$

## REFERENCES


Agostinelli, S., et al., 2003, Geant4—a simulation toolkit. Nuclear Instruments and Methods in Physics Research A 506, 250–303; doi: 10.1016/S0168-9002(03)01368-8

Allison, J., et al., 2006, Recent developments in GEANT 4. IEEE TRANSACTIONS ON NUCLEAR SCIENCE, 53, 270-278; doi: 10.1109/TNS.2006.869826

Allison, J., et al., 2016, Geant4 Developments and Applications. Nuc. Instr. Methods A835, 186–225; doi: 10.1016/j.nima.2016.06.125

Biermann, V. L., Haxe, O., Schulter, A., 1951, Neutrale Ultrastrahlung von der Sonne. Zeitschrift für Naturforschung 6a, 47-48; doi: 10.1515/zna-1951-0107

Bramblett, R., Ewing, R. I., Bonner, T. W., 1960, A new type of neutron spectrometer. Nuclear Instruments and Methods, 9, 1-12; doi: 10.1016/0029-554X(60)90043-4

Brant, A., Buchanan, D., Mcclory, J., Dowben, P., Adamiv, V., Burak, Y., & Halliburton, L., 2013. EPR identification of defects responsible for thermoluminescence in Cu-doped lithium tetraborate ($Li_2B_4O_7$) crystals. Journal of Luminescence, 139, 125-131. doi:10.1016/j.jlumin.2013.02.023

Caruso, A. N., 2010, The physics of solid-state neutron detector materials and geometries. J. Physics: Condensed Matter 22, 443201; doi:10.1088/0953-8984/22/44/443201

Chadwick, M.B., et al., 2006, ENDF/B-VII.0: Next Generation Evaluated Nuclear Data Library for Nuclear Science and Technology, 2006, Nuclear Data Sheets, 107, 2931; https://e-reports-ext.llnl.gov/pdf/339260.pdf

Chupp, E. L., et al., 1982, A direct observation of solar neutrons following the 0118 UT flare on 1980 June 21. Astrophysical Journal, 263, L95; doi: 10.1086/183931

Chupp, E. L., Debrunner, H., Flueckiger, E., Forrest, D. J., Golliez, F., Kanbach, G., 1987, Solar neutron emissivity during the large flare on 1982 June 3. Astrophysical Journal, 318, 913; doi: 10.1086/165423

Clem, J. M, De Angelis, G., Goldhagen, P., Wilson, J. W., 2004, "New Calculations of the Atmospheric Cosmic Radiation Field-results For Neutron Spectra. Radiation Protection Dosimetry, 110, 423-428 doi:10.1093/rpd/nch175

Echeverria, E., et al., 2016, Semiconducting boron carbides with better charge extraction through the addition of pyridine moieties. J. Physics D, 49, 355302; doi:10.1088/0022-3727/49/35/355302

Echeverría, E., Dong B., Liu, A., Wilson, E. R., Peterson, G., Nastasi, M., Dowben, P. A., Kelber, J. A., 2017. Strong binding at the gold (Au) boron carbide interface, Surface

and Coatings Technology, 314, 51; doi: 10.1016/j.surfcoat.2016.08.081

Feldman, W. C., Asbridge, J. R., Bame, S. J., Gosling J. T., 1978, Long-term variations of selected solar wind properties - IMP 6, 7, and 8 results. Journal of Geophysical Research: Space Physics, 83, 2177; doi: 10.1029/JA083iA05p02177

Feldman, W.C., et al., 2010, Evidence for extended acceleration of solar flare ions from 1–8 MeV solar neutrons detected with the MESSENGER Neutron Spectrometer, 2010, Journal of Geophysical Research: Space Physics, 115(A1), A01102; doi: 10.1029/2009JA014535

Forrest, D.J. et al, 1982, Evidence for impulsive ion acceleration during the 0312 UT flare of 1980 June 7. International Cosmic Ray Conference, 17th, Paris, France, July 13-25, 1981, Gif-sur-Yvette, Essonne, France, Commissariat a l'Energie Atomique, Bundesministerium für Forschung und Technologie, Conference Papers. 10. (A82-30442 14-88), 5-8

Goldstein, B. E., et al., 1996, ULYSSES plasma parameters: latitudinal, radial, and temporal variations. Astronomy and Astrophysics, 316, 296

Goorley, T., et al., 2012, Initial MCNP6 Release Overview, Nuclear Technology, 180, 298–315; doi: 10.13182/NT11-135

Goorley, T., et al., 2016, Features of MCNP6. Annals of Nuclear Energy, 87, 772-783; doi: 10.1016/j.anucene.2015.02.020

Holman, G.D., 2000, Particle Acceleration in Large-Scale DC Electric Fields. ASP Conf. Ser., Ramaty R., Mandzhavidze N., eds, Astron. Soc. Pac, San Francisco, 206, 135

Hoshor, C. et al., 2015, A portable and wide energy range semiconductor-based neutron spectrometer, Nuclear Instruments and Methods in Physics A, 803, 68; doi: 0.1016/j.nima.2015.08.077

Hoshor, C., et al., 2017, Real-time neutron source localization and identification with a hand-held, volumetrically-sensitive, moderating-type neutron spectrometer. Nuclear Instruments and Methods in Physics A, 866, 252; doi: 10.1016/j.nima.2017.05.033

Hoyle, F., 1946, The synthesis of the elements from hydrogen. Monthly Notices of the Royal Astronomical Society, 106, 343; doi: 10.1093/mnras/106.5.343

Hoyle, F., 1954, On Nuclear Reactions Occurring in Very Hot STARS. I. The Synthesis of Elements from Carbon to Nickel. Astrophysical Journal Supplements, 1, 121; doi: 10.1086/190005

Ilie, C. C., et al., 2018, Inkjet printable-photoactive all inorganic perovskite films with long effective photocarrier lifetimes. Journal of Physics Condensed Matter, 30, 13LT02; doi: 10.1088/1361-648X/aab986

Koga, K., Goka, T., Matsumoto, H., Muraki, Y., Masuda, K., Matsubura, Y., 2001, Development of the fiber neutron monitor for the energy range 15-100 MeV on the International Space Station (ISS). Radiation Measurements, 33, 287

Koga, K., Goka, T., Matsumoto, H., Obara, T., Muraki, Y., Yamamoto, T., 2011, Measurement of high-energy neutrons at ISS by SEDA-AP. Astrophysics and Space

Sciences Transactions, 7, 411; doi:10.5194/astra-7-411-2011

Kuznetsov, S.N., Kurt, V. G., Myagkova, B., Yushkov, B. Yu., Kudela, K., 2006, Gamma-ray emission and neutrons from solar flares recorded by the SONG instrument in 2001-2004, Solar System Research, 40, 104; doi: 10.1134/S0038094606020031

Kuznetsov, S. N., Kurt, V., Yushkov, B. Yu., Kudela, K., Galkin, V. I., 2011, Gamma-Ray and High-Energy-Neutron Measurements on CORONAS-F during the Solar Flare of 28 October 2003. Solar Physics, 268, 175; doi: 10.1007/s11207-010-9669-2

Lawrence, D. J., Feldman, W. C., Goldsten, J. O., Peplowski, P. N., Rodgers, D. J., Solomon, S. C., 2014, Detection and characterization of 0.5–8 MeV neutrons near Mercury: Evidence for a solar origin. J. Geophysical Research: Space Physics, 119, 5150; doi: 10.1002/2013JA019037

Leer, E., Holzer, T.E., Flå, T., 1982, Acceleration of the solar wind. Space Science Reviews, 33, 161; doi: 10.1007/BF00213253

Li, X., Selesnick, R., Schiller, Q., Zhang, K., Zhao, H., Baker, D. N., Temerin, M. A., 2017. Measurement of electrons from albedo neutron decay and neutron density in near-Earth space. Nature, 552, 382; doi: 10.1038/nature24642

Masuda, S., Kosugi, T., Hara, H., Tsuneta, S., Ogawara, Y., 1994, A loop-top hard X-ray source in a compact solar flare as evidence for magnetic reconnection. Nature, 371, 495

McConnell, M., Bennett, K., Forrest, D., Hanlon, L., Ryan, J., Schönfelder, V., Swanenburg, B. N., Winkler, C., 1993, Comptel observations of solar flare gamma-rays. Advances in Space Research, 13, 245; doi: 10.1016/0273-1177(93)90485-T.

McConnell, M., 1994, An overview of solar flare results from COMPTEL. AIP Conf. Proc. Ryan J. M., Vestramd W. T., eds, 294, 21; doi: 10.1063/1.45193

Muraki, Y. & Shibata, S., 1996, Solar neutrons on May 24th, 1990. in AIP Conf. Proc., 374, 256; doi: 10.1063/1.50961

Muraki, Y., Koga, K., Goka, T., Matsumoto, H., Obara, T., Okudaira, O., Shibata, S., Yamamoto, T., 2012, Measurement by FIB on the ISS: Two Emissions of Solar Neutrons Detected?. Advances in Astronomy, 2012, 379304; doi: 10.1155/2012/379304

Murphy, R. J., Share, G. H., DelSignore, K. W., Hua, X.-M., 1999, Surprisingly Intense Neutron Emission from a Flare behind the Limb of the Sun. Astrophysical Journal, 510, 1011; doi: 0004-637X/510/2/1011

Patra, G., Tyagi, M., Desai, D. G., Tiwari, B., Sen, S., Gadkari, S. C., 2012, Photo-luminescence properties of Cu and Ag doped $Li_2B_4O_7$ single crystals at low temperatures. Journal of Luminescence, 132, 1101; doi: 10.1016/j.jlumin.2011.12.005

Patra, G., Singh, S. G., Tiwari, B., Sen, S., Desai D. G., Gadkari S. C., 2013, Thermally stimulated luminescence process in copper and silver co-doped lithium tetraborate single crystals and its implication to dosimetry. Journal of Luminescence, 137, 28; doi: 10.1016/j.jlumin.2012.12.007

Peterson, G. G., Su, Q., Wang, Y., Ianno, N. J., Dowben, P. A., Nastasi, M., 2018, Improved a-$B_{10}C_{2+x}H_y$/Si p-n heterojunction

performance after neutron irradiation. Journal of Vac. Sci. Technol. B, Nanotechnology and Microelectronics: Materials, Processing, Measurement, and Phenomena 36, 011207; doi: 10.1116/1.5008999

Petschek, H.E., 1964, Magnetic Field Annihilation. in Proc. AAS-NASA Symp., Hess W. N., ed, 50, 425

Rank, G., et al., 1996, Extended γ-ray emission in solar flares. in AIP Conf. Proc. 374, 219

Rawat, N., et al., 2012, TL and OSL studies on lithium borate single crystals doped with Cu and Ag. Journal of Luminescence, 132, 1969; doi: 10.1016/j.jlumin.2012.03.008

Ryan, J. M., 2000, Long-Duration Solar Gamma-Ray Flares, Space Science Reviews, 93, 581; doi:10.1023/A:1026547513730

Ryan, J. M., et al., 1994, Neutron and gamma-ray measurements of the solar flare of 1991 June 9. in AIP Conf. Proc., Ryan J. M., Vestramd W. T., eds, 294, 89; doi: 10.1063/1.45205

Ryan, J. M., McConnell, M. M., 1996, COMPTEL solar flare measurements. in AIP Conf. Proc. 374, 200; doi: 10.1023/A:1026547513730

Share, G. H., Murphy, R. J., Tylka, A. J., Dennis, B. R., Ryan, J. M., 2015, Misidentification of the source of a neutron transient1detected by MESSENGER on 2011 June 4. Journal of Geophysical Research: Space Physics, 120, 1; doi: 10.1002/2014JA020663

Shea, M. A., Smart, D. F., Pyle, K. R., 1991, Direct solar neutrons detected by neutron monitors on 24 May 1990, Geophysical Research Letters, 18, 1655

Shibata, K., 1998, Evidence of Magnetic Reconnection in Solar Flares and a Unified Model of Flares. Astrophysics and Space Science, 264, 129; doi: 10.1023/A:1002413214356

Tiwari, B., Rawat, N. S., Desai, D. G., Singh, S. G., Tyagi, M., Ratna, P., Gadkari, S. C., Kulkarni, M. S., 2010, Thermoluminescence studies on Cu-doped $Li_2B_4O_7$ single crystals, Journal of Luminescence, 130, 2076; doi: 10.1016/j.jlumin.2010.05.030

Wang, Y.-M., 2010, On the Relative Constancy of the Solar Wind Mass Flux at 1 AU. Astrophysical Journal, 715, L121; doi: 10.1088/2041-8205/715/2/L121

Wiegel, B., Alevra, A. V., Matzke, M., Schrewe, U. J., Wittstock, J. 2002, Spectrometry using the PTB neutron multisphere spectrometer (NEMUS) at flight altitudes and at ground level, Nuclear Instruments and Methods in Physics Research A 476, 52–57; doi: 10.1016/S0168-9002(01)01387-0

Yokoyama, T., Shibata, K., 1998, Two-dimensional Magnetohydrodynamic Simulation of Chromospheric Evaporation in a Solar Flare Based on a Magnetic Reconnection Model. Astrophysical Journal, 494, L113